Lithuanian Journal of Physics
Vol. **63**, No. 2, pp. 73–84 (2023)
ISSN 1648-8504 eISSN 2424-3647
DOI: https://doi.org/10.3952/physics.2023.63.2.4

# A COMPUTATIONAL STUDY OF THE ELECTRONIC AND THERMOELECTRIC PROPERTIES OF METAL HALIDE CUBIC PEROVSKITES $CsBX_3$ (B = Ge, Sn, Pb AND X = Cl, Br, I)

**M. Zemzemi**

*Laboratory of Physics of Materials and Nanomaterials Applied to Environment, Faculty of Sciences of Gabès, University of Gabès, Erriadh City, Zrig, 6072 Gabès, Tunisia*
Email: mzemzemi@gmail.com

Received 17 September 2022; revised 29 November 2022; accepted 6 December 2022

Metal halide perovskites have received a tremendous interest recently in new applications. Photovoltaic, diverse photonic and optoelectronic applications of these materials are in full expansion, but thermoelectricity also instigates a great interest. In this work, we will focus on the thermoelectric properties of a particular material family of metal halide cubic perovskites $CsBX_3$ (B = Ge, Sn, Pb and X = Cl, Br, I). The structural and electronic properties of $CsBX_3$ are computed using first-principles calculations based on the density functional theory which allows calculating equilibrium lattice parameters, band structures, the nature (direct/indirect) and value of the band gap. These studied compounds are semiconductors with direct band gap energy. We have also detected the effect of replacement of halogen and metal cation atoms with other halogen and metal cation atoms on electronic and thermoelectric properties. Boltzmann transport calculations are carried out to explore their thermoelectric properties like the Seebeck coefficient, electrical conductivity and power factor. Large values of the Seebeck coefficient and the power factor obtained for these compounds indicate that these compounds can be used for thermoelectric devices. Our theoretical analysis of the electronic and thermoelectric properties of these compounds suggests that $CsSnBr_3$ and $CsGeBr_3$ are the best Pb-free inorganic metal halide semiconductor for a high thermoelectric performance.

**Keywords:** metal halide cubic perovskites, thermoelectric properties, electronic properties, density functional theory, Boltzmann transport theory

## 1. Introduction

Thermoelectric materials and devices, using small temperature differences to generate electricity, exhibit a great potential to provide the continuous power supply for wearable and implantable electronics [1]. Searching and identifying of thermoelectric materials with a higher efficiency than available remain a challenge. The strategies and approaches for enhancing the thermoelectric properties are based on improving the performance of existing materials, researching new materials using doping, exploiting new nanoscale materials, such as graphene [2], and creating new structures based on heterojunctions [3].

Material halide perovskites have attracted a great interest due to their fascinating physical and chemical properties, such as a controllable particle size, reduced dimensionality and adjustable chemical composition. They possess a typical perovskite crystal structure of $ABX_3$, where A is an inorganic or organic cation, B is a metal cation, and X is a halide anion [4]. This structure provides the ability to perform a large number of atom replacements, which offers an extensive amount of possible combinations of halide perovskites [5]. This flexibility has produced astonishing results in this field [4]. Material halide perovskites are also known for their high chemical stability and environmental friendliness [6]. There has been a significant progress in the synthesis, processing and characterization of this family of materials. Nanostructures of metal halide perovskites have received an escalating interest, including nanocrystals,

nanowires and quantum wells [7]. Intense research activities have been focused on halide perovskites semiconductors, which are being developed for solar cells [8], lasers [9], water splitting [10] and laser cooling [11]. Compared to the most conventional semiconductors, metal halide perovskites take up a considerable place as photocatalysts for $CO_2$ reduction [12]. They exhibit unique photophysical and optoelectronic properties and they have the additional advantages of a low cost and an easy scale-up synthesis [13, 14]. These properties confirm not only the great potential of material halide perovskites but also a broad field of study that remains untapped. Searching and identifying these materials with a higher thermoelectric efficiency than available at present is a challenge. However, a resurgence of interest in thermoelectrics began when theoretical predictions suggested that thermoelectric efficiency could be greatly enhanced through nanostructural engineering, which led to experimental efforts to demonstrate the proof-of-principle and high-efficiency materials [15, 16].

Thermoelectric devices can be used to generate electricity, measure temperature or change the temperature of objects. However, most of these devices have relied on expensive and toxic materials, as well as intensive-energy manufacturing. Finding efficient thermoelectric materials remains critical to the development of clean and renewable energy conversion technologies. To optimize and build a competitive perovskites-based thermoelectric device, fundamental studies of the electronic structure and thermoelectric properties are necessary and of great significance. The recent progress regarding a better exploitation of the new properties of metal halide perovskites is in understanding how chemical compositions contribute to the electronic structure and chemical stability [17–20].

In this work, we present our recent results, which aim at clarifying the relationship between the structural, electronic and thermoelectric properties of metal halide perovskites $CsBX_3$ (B = Ge, Sn, Pb and X = Cl, Br, I). First, we will calculate the structural and electronic properties within the density function theory (DFT) framework. Second, using Boltzmann's equations coupled with DFT, the investigation of thermoelectric properties has been illustrated through a calculation of the Seebeck coefficient, electrical conductivity and power factor. Third, we have made emphasis on examining the relation between the electronic and thermoelectric properties of $CsBX_3$ chemical composition.

## 2. Computational details

*Ab initio* is an adapted technique for the realistic simulation of structural, electronic, magnetic and optical properties from the first principles. First-principles methods, based on DFT [21] and implemented in the Abinit simulation package [22], were used to investigate the structural and electronic properties of metal lead halide cubic perovskite. An essential element in every DFT calculation is the usage of effective core potentials for atoms, called pseudopotentials. In this work, Garrity–Bennett–Rabe–Vanderbilt (GBRV) pseudopotentials [23] and projector augmented wave (PAW) potentials have been used [24]. The GBRV pseudopotentials represent the norm-conserving class of pseudopotentials, while the PAWs are obtained with the PAW transformation and provide much gain in the efficiency of the calculations. The exchange-correlation energy was obtained by using the generalized gradient approximation (GGA) of Perdew–Berke–Ernzerhof (PBE) [24]. The kinetic energy cutoff for the plane wave is chosen as 500 eV. The Monkhorst–Pack scheme [25] is used to sample the Brillouin zone by $10 \times 10 \times 10$ special $k$-points. Concerning the thermoelectric properties, calculations require a dense $k$-mesh of $40 \times 40 \times 40$ $k$-points. Energy and force convergence criteria of $10^{-5}$ eV and $3 \times 10^{-2}$ eV/Å, respectively, were used in all calculations.

First, we examine the structural stability by the optimization of lattice parameters and atomic positions. Optimal lattice parameters for all compounds were obtained with the equation of state calculations on the primitive cell [26]. Second, we calculate the electronic properties of all compounds in their equilibrium structures. Third, the thermoelectric properties have been investigated employing first-principles calculations of the electronic properties followed by the calculations of transport coefficients based on the Boltzmann transport equation (BTE). This theory has been successfully used to study and/or to predict the performance of many thermoelectric materials. All thermoelectric properties reported herein were calculated using the BoltzTraP code [27]. The transport properties such as the Seebeck coefficient, electrical conductivity and electronic thermal conductivity were calculated

using this code. Before presenting the calculated results, we present briefly the expressions of different thermoelectric coefficients [28]. The electrical conductivity $\boldsymbol{\sigma}$ is computed as

$$\sigma = e^2 \int \Sigma(\varepsilon) \left( -\frac{\partial f_o}{\partial \varepsilon} \right) \mathrm{d}\varepsilon. \quad (1)$$

The Seebeck coefficient $S$ used here is

$$S = \frac{e}{T\sigma} \int \Sigma(\varepsilon)\,(\varepsilon - \mu) \left( -\frac{\partial f_o}{\partial \varepsilon} \right) \mathrm{d}\varepsilon. \quad (2)$$

The electronic thermal conductivity $\boldsymbol{\kappa}_o$ can be calculated from the equation

$$\kappa_o = \frac{1}{T} \int \Sigma(\varepsilon)\,(\varepsilon - \mu)^2 \left( -\frac{\partial f_o}{\partial \varepsilon} \right) \mathrm{d}\varepsilon, \quad (3)$$

where $e$ is the electron charge, $\boldsymbol{\mu}$ is the chemical potential, $f_o$ is the Fermi distribution function, and $\Sigma(\boldsymbol{\varepsilon})$ is the transport distribution function. $\Sigma(\boldsymbol{\varepsilon})$ is given by

$$\Sigma(\varepsilon) = \sum_{\vec{k}} \tau(\vec{k}) \upsilon^2(\vec{k}) \delta(\varepsilon - \varepsilon(\vec{k})), \quad (4)$$

where $\upsilon(\vec{k})$ is the group velocity of the carriers with the wave vector $\vec{k}$, $\boldsymbol{\tau}(\vec{k})$ is the carrier lifetime, and $\boldsymbol{\varepsilon}(\vec{k})$ is the dispersion relation for the carriers. The electronic thermal conductivity is proportional to the electrical conductivity as established by the Wiedemann–Franz law: $\boldsymbol{\kappa}_o = L\sigma T$, where $L$ denotes the Lorenz number.

## 3. Results and discussion

### *3.1. Structural properties*

Temperature-dependent structural phase transitions are very common in perovskites. Different $CsBX_3$ type materials have been found in multiple crystallographic phases at different temperatures. We detect common phases being cubic, tetragonal and orthorhombic. However, the cubic phase is the most common phase among the $CsBX_3$ type materials. Also, the cubic perovskite phase is widely accepted as a room-temperature phase which is generally found at a higher temperature compared to other existing phases, therefore the cubic phase is also called the high-temperature phase [29]. $CsBX_3$ (B = Ge, Sn, Pb and X = Cl, Br, I) adopted a cubic perovskite crystal structure, with the space group Pm $\bar{3}$m (No. 221). The perovskite structure consists of two cations of different size and one anion. The B-cation has a 6-fold coordination with the X anions forming an octahedron which is surrounded by a scaffold of Cs-cations. $CsBX_3$ has five atoms per unit cell. The five atoms taken into account are located as follows: Cs atom resides at the 1a Wyckoff position (0, 0, 0), B atom is located at the 1b Wyckoff position (0.5, 0.5, 0.5), and X 3 atoms are at the 3c Wyckoff position (0, 0.5, 0.5) [30]. Figure 1 shows the perovskite structure arrangement of a unit cell in the cubic symmetry. In this study, we have first performed geometry optimization calculations of $CsBX_3$ using the Birch–Murnaghan equation of state. This equation is used to plot the calculated total energy of each unit cell in a compound against the corresponding calculated volumes. The equilibrium lattice constants for each compound are given in Table 1.

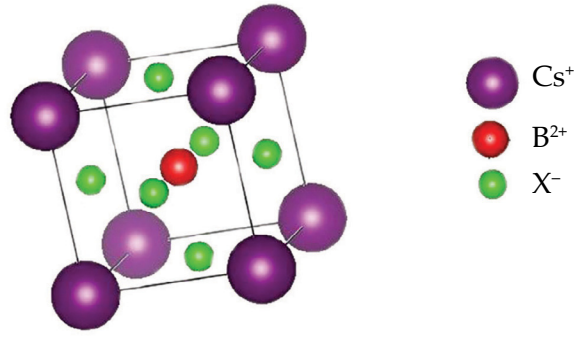


Fig. 1. Unit cells of the considered metal halide cubic perovskites $CsBX_3$ (B = Ge, Sn, Pb; X = Cl, Br, I), where $Cs^+$, $B^{2+}$ and $X^-$ occupy the corner, body centered and face centered positions, respectively.

Table 1. Calculated lattice constants of $CsBX_3$ (B = Ge, Sn, Pb and X = Cl, Br, I) with experimental and other DFT calculated values.

| Compounds | Present work | Other calculations | Experiment |
|---|---|---|---|
| $CsGeCl_3$ | 5.34 | 5.16 [31] | 5.47 [32] |
| $CsGeBr_3$ | 5.60 | 5.55 [31] | 5.35 [33] |
| $CsGeI_3$ | 5.99 | 5.78 [31] | 6.05 [32] |
| | | | |
| $CsSnCl_3$ | 5.63 | 5.61 [34] | 5.56 [33] |
| $CsSnBr_3$ | 5.89 | 5.87 [34] | 5.79 [35] |
| $CsSnI_3$ | 6.28 | 6.25 [v4] | 6.21 [36] |
| | | | |
| $CsPbCl_3$ | 5.73 | 5.73 [37] | 5.62 [38] |
| $CsPbBr_3$ | 6.00 | 5.87 [39] | 5.85 [40] |
| $CsPbI_3$ | 6.39 | 6.39 [37] | 6.24 [38] |

### *3.2. Electronic properties*

After calculating the optimized structure of different compounds, density functional calculations using the GGA-PBE approximation were further carried out to calculate the electronic properties. The electronic band structures are calculated to obtain the band gap of all compounds of $CsBX_3$ (B = Ge, Sn, Pb and X = Cl, Br, I). Figure 2 displays the calculated band structures along the high symmetry path of *k*-points Γ → X → M → R → Γ in the Brillouin zone. From our calculated results, it is clear that all these compounds are direct band gap materials (Fig. 2). This property is also confirmed experimentally [41]. The maxima of their valence bands and the minima of conduction band are separated by R–R symmetric points in the Brillouin zone. The energy band gap values for $CsBX_3$ are listed in Table 2. A higher band gap is observed for the compounds containing lighter halogen atoms (X = Cl). The higher electro-negativity of a halogen (Cl > Br > I) corresponds to a larger gap energy. So, this reflects the halogen-p character in the valence band maximum (Fig. 3). When we change the B atoms, we also observe that the energy gap decreases. This is explained by the fact that the decreasing trend results from the trend in the size of the atoms and hence bond lengths. Hence, the shorter the bond length is, the stronger the hybridization width and the smaller the band gap are. However, an exception is observed in the case of replacement of Pb by Sn and Ge. The Ge containing compounds have higher electronic band gaps than Sn containing compounds, the electronic states of the conduction band slightly shift towards the high energy and this is very common for this group of compounds [42].

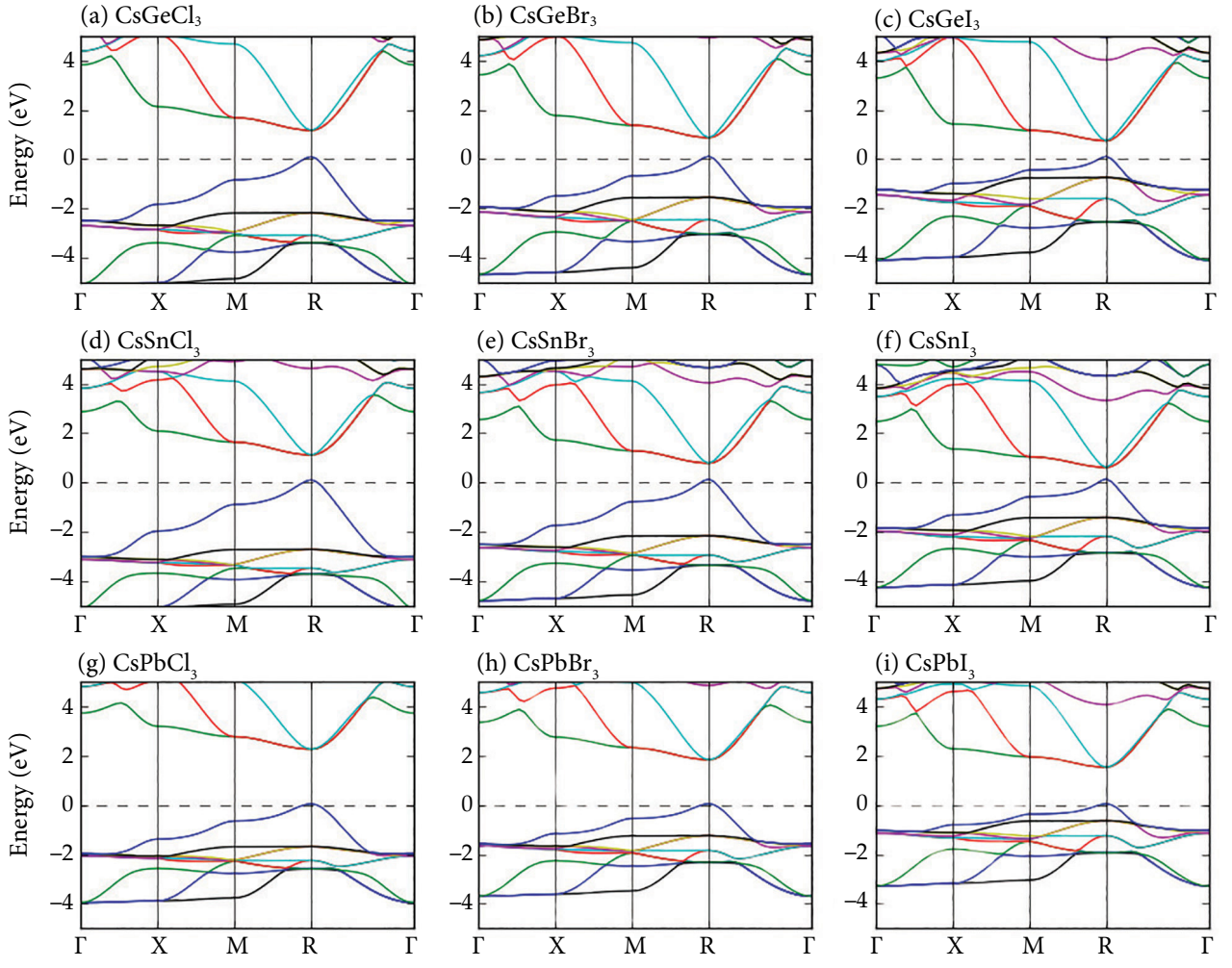


Fig. 2. The electronic band structures and the density of states (DOS) of $CsBX_3$ (B = Ge, Sn, Pb; X = Cl, Br, I) calculated by the GGA-PBE exchange–correlation functional. The valence band maximum was set to 0 eV.

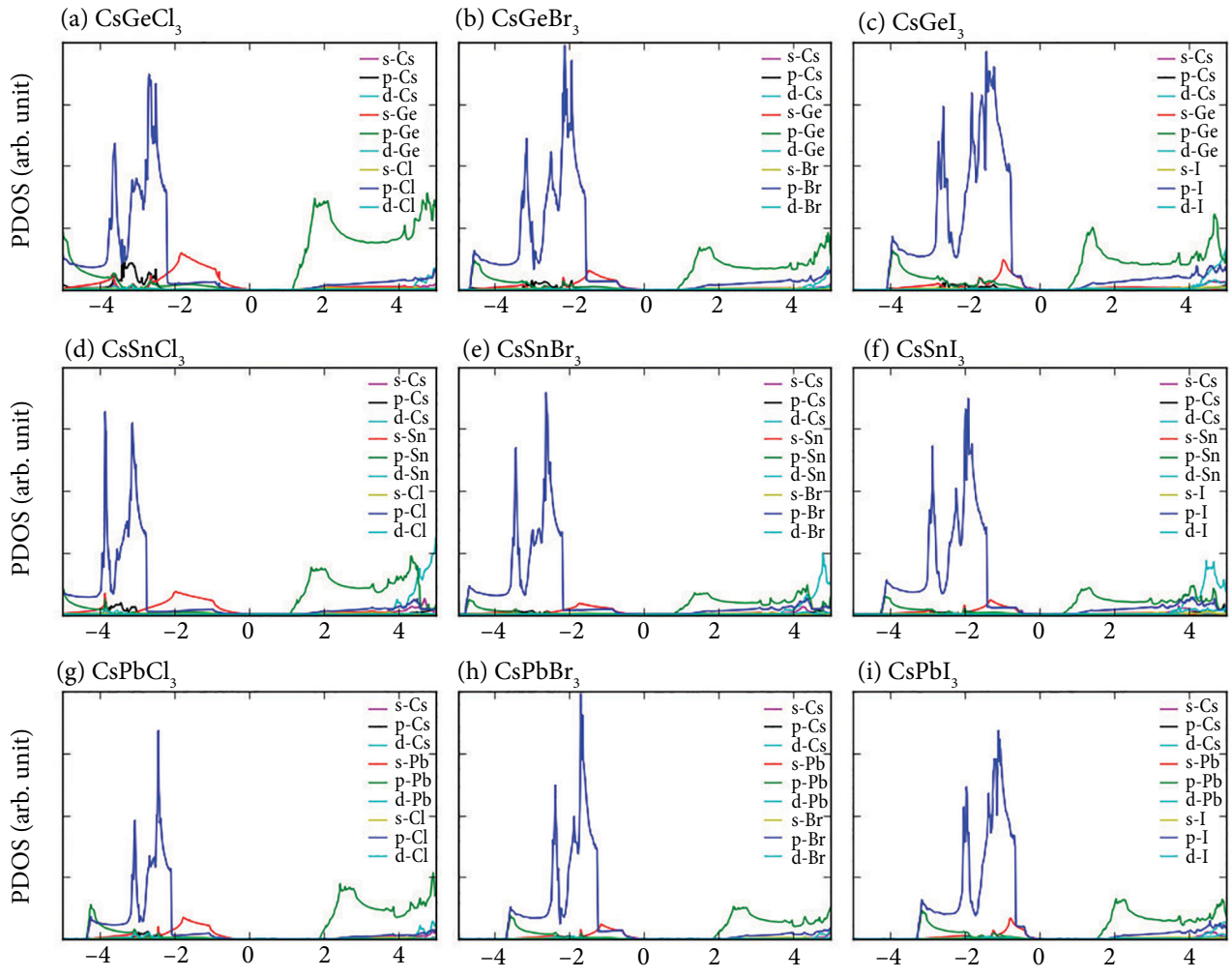


Fig. 3. Partial density of the states (POS) of $CsBX_3$ (B = Ge, Sn, Pb; X = Cl, Br, I) calculated by the GGA-PBE exchange–correlation functional.

The study of the electronic band structure suggests that the pattern of the band structure is slightly affected by replacement of a halogen atom with other halogen atoms. Due to this characteristic, metal halide perovskites are suitable to be used in light emitting diodes (LED) as the band gap of these materials can easily be tuned by changing the halogen contents while the other properties remain almost the same.

Further explanation of the nature of the electronic band gap energy of $CsBX_3$ compounds is carried out through the partial density of states (PDOS). The PDOS, explaining the contribution of each orbital to the atomic bond, is plotted in Fig. 3. This confirms that in all compounds the conduction band minimum is mainly contributed by the p orbital of B atoms, such as 6p from Pb, 5p from Sn and 4p from Ge [43]. The upper valence band consists mainly of B s states but near the top we can

Table 2. Calculated band gap energy of cubic perovskites $CsBX_3$ (B = Ge, Sn, Pb and X = Cl, Br, I) with experimental and other DFT calculated values using the generalized gradient approximation (GGA) of Perdew–Berke–Ernzerhof (PBE). All these calculation results are at 0 K.

| Compound | Present work | Other calculations | Experiment |
|---|---|---|---|
| $CsGeCl_3$ | 1.20 | 0.98 [43] | 3.40 [44] |
| $CsGeBr_3$ | 0.90 | 0.70 [43] | 2.39 [44] |
| $CsGeI_3$ | 0.75 | 0.58 [43] | 1.63 [45] |
| | | | |
| $CsSnCl_3$ | 1.15 | 0.90 [43] | 2.9 [46] |
| $CsSnBr_3$ | 0.8 | 0.60 [43] | 1.75 [31] |
| $CsSnI_3$ | 0.6 | 0.40 [43] | 1.3 [47] |
| | | | |
| $CsPbCl_3$ | 2.30 | 2.20 [43] | 3.13 [48] |
| $CsPbBr_3$ | 1.80 | 1.80 [43] | 2.47 [48] |
| $CsPbI_3$ | 1.60 | 1.48 [43] | 1.85 [48] |

recognize a sizable X p component. These are antibonding combinations of X p and B s. The contribution of Cs orbitals in the upper valence band and conduction band minimum is small.

### *3.3. Thermoelectric properties*

Many experimental and theoretical studies predict metal halide perovskites as promising materials for thermoelectric applications [18, 48]. These compounds present unique opportunities for thermoelectricity through manipulating the cation and halide compositions. This theoretical work focuses on understanding the thermoelectric properties of $CsBX_3$ (B = Ge, Sn, Pb and X = Cl, Br, I) including the Seebeck coefficient, electrical conductivity and power factor. We will present the relationship between the chemical composition and thermoelectric properties.

The Seebeck coefficient *S* is a measure of the magnitude of an induced thermoelectric voltage in response to a temperature gradient. The magnitude, sign and dependence on the temperature of *S* are important factors to select the high-performance thermoelectric materials. Figure 4 shows *S* of the $CsBX_3$ plots versus temperature. For all the compounds, *S* takes positive values in the entire considered temperature range, which justifies the p-type of these compounds. By analyzing the curves in Fig. 4, we can see that, among all the compounds $CsBX_3$, the value of the Seebeck coefficient is higher for those containing a chlorine anion, and lower for bromine, while iodine yields the lowest values. This finding is also confirmed by the *S* values listed in Table 3, which displays different compounds at the temperatures of 300 and 600 K. It can be clearly seen from Fig. 4, for all compounds $CsBX_3$ containing chlorine, that *S* increases with temperature over the entire range between 200 and 800 K. For the other compounds $CsBX_3$ (B = Ge, Sn and X = Br, I), beyond 200 K, *S* increases slightly, however beyond 600 K, it decreases nearly linearly as the temperature is raised, while that of the $CsPbX_3$ continues increasing with temperature. Our results suggest that the $CsGeX_3$ compounds may enhance the thermoelectric potential, measured by the Seebeck coefficient, specifically, for $CsGeCl_3$ which is desirable. The $CsGeCl_3$ compound possesses the largest Seebeck coefficient that is 402 $\mu VK^{-1}$ at 300 K and increases to 520 $\mu VK^{-1}$ at 600 K.

The understanding of electrical properties of many functional materials including metal halide perovskites is a challenge. However, expectations from the effect of atom replacement of halogen and metal cation atoms by other halogen and metal cation atoms on the electrical transport properties of $CsBX_3$ have not yet been clearly confirmed experimentally. Our theoretical study based on DFT coupled with Boltzmann's theory can help to understand the relationship between the electrical conductivity and atomic composition. The curves in Fig. 5 illustrate the temperature dependence of $CsBX_3$ electrical conductivity in a range from 200 to 800 K. These curves show that $CsBX_3$ compounds exhibit the semiconductor behaviour with a decreasing electrical conductivity over the majority of the temperature range. They also show that whatever the anion,

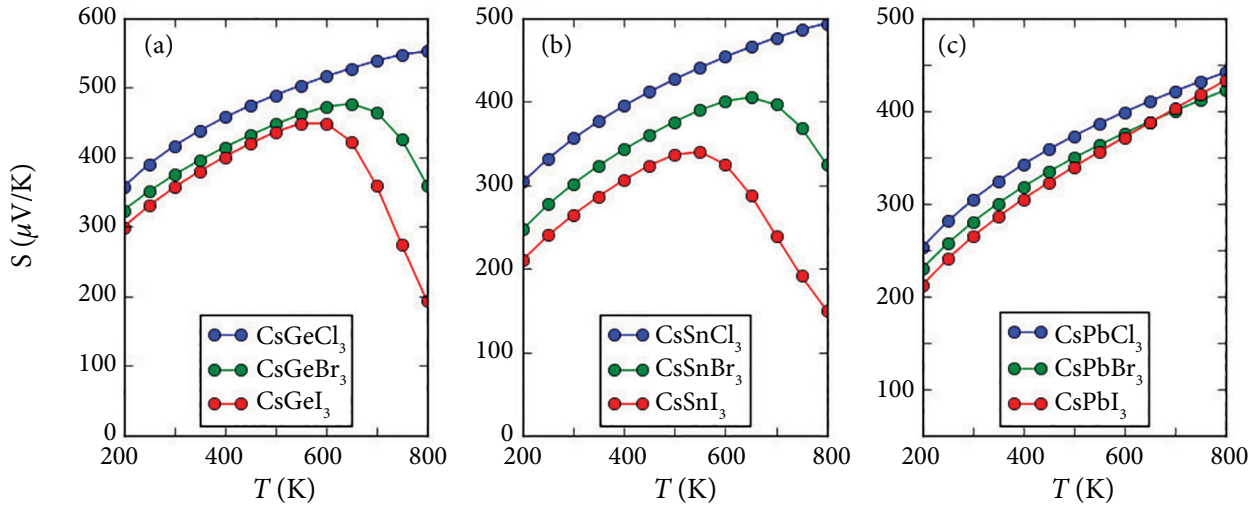


Fig. 4. Temperature-dependent Seebeck coefficient of $CsBX_3$ (B = Ge, Sn, Pb; X = Cl, Br, I).

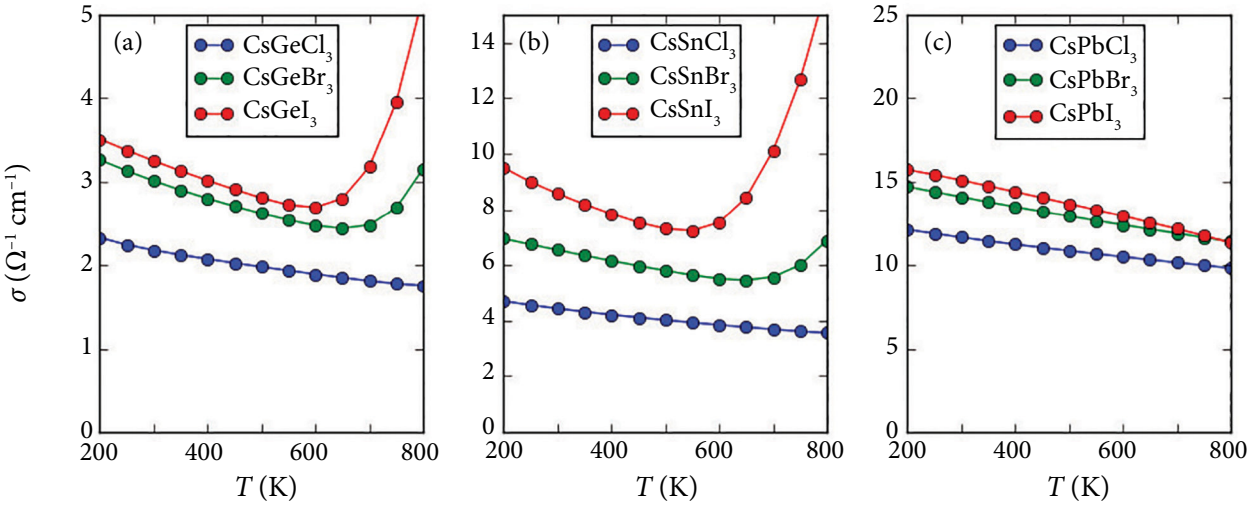


Fig. 5. Temperature-dependent electrical conductivity of $CsBX_3$ (B = Ge, Sn, Pb; X = Cl, Br, I).

the conductivity of the $CsBI_3$ compounds is always the highest. Note that in the considered temperature range, the electrical conductivity decreases in the order: $CsBI_3 \rightarrow CsBBr_3 \rightarrow CsBCl_3$. In Fig. 5(a, b), two ranges can be identified in which the change of electrical conductivity with temperature exhibits different slopes. From 200 to 600 K, the electrical conductivity decreases by showing a semiconductor nature of the compounds. Beyond the temperature of 600 K, a significant increase is observed which is explained by a modification in the mobility of the electrons that corresponds to a change in the halide anions (iodine and bromine). As regards chlorine and lead-based compounds, the electrical conductivity is uniformly decreasing over the entire temperature range. Table 3 confirms that lead-based compounds have the highest electrical conductivity. $CsPbI_3$ has a value that decreases from 15.3 to 13.3 $\Omega^{-1}$ cm$^{-1}$ between 300 to 600 K. When we replace the atoms of Pb by Ge or Sn, we observe also that $CsSnX_3$ exhibits a slightly higher electrical conductivity than $CsGeX_3$. This result proves that the electrical conductivity can be increased by several orders of magnitude with the metal, and also with the type of halogen.

The efficiency of most thermoelectric devices is proportional to the figure of merit $zT = \sigma S^2 T / (\kappa_o + \kappa_l)$, where $S$ is the Seebeck coefficient, $\boldsymbol{\sigma}$ is the electrical conductivity, $\kappa_o$ is the electronic thermal conductivity, and $\kappa_l$ is the lattice thermal conductivity. Attempts are being made

Table 3. Summary of thermoelectric properties like the Seebeck coefficient, electrical conductivity and power factor of $CsBX_3$ (B = Ge, Sn, Pb and X = Cl, Br, I) at temperatures 300 and 600 K.

| | $T$ = 300 K | | | $T$ = 600 K | | |
|---|---|---|---|---|---|---|
| Compound | $S$, $\mu$V/K | $\Sigma$, $\Omega^{-1}$ cm$^{-1}$ | PF, $\mu$W cm$^{-1}$ K$^{-2}$ | $S$, $\mu$V/K | $\Sigma$, $\Omega^{-1}$ cm$^{-1}$ | PF, $\mu$W cm$^{-1}$ K$^{-2}$ |
| $CsGeCl_3$ | 420 | 2.18 | 0.38 | 520 | 1.93 | 0.52 |
| $CsGeBr_3$ | 375 | 3.00 | 0.42 | 472 | 2.50 | 0.55 |
| $CsGeI_3$ | 355 | 3.20 | 0.40 | 450 | 2.68 | 0.54 |
| | | | | | | |
| $CsSnCl_3$ | 357 | 4.36 | 0.55 | 455 | 4.00 | 0.82 |
| $CsSnBr_3$ | 303 | 6.54 | 0.60 | 400 | 5.63 | 0.90 |
| $CsSnI_3$ | 264 | 8.54 | 0.59 | 321 | 7.45 | 0.76 |
| | | | | | | |
| $CsPbCl_3$ | 307 | 11.50 | 1.08 | 397 | 10.60 | 1.67 |
| $CsPbBr_3$ | 280 | 13.93 | 1.09 | 375 | 12.42 | 1.74 |
| $CsPbI_3$ | 260 | 15.30 | 1.03 | 367 | 13.03 | 1.75 |

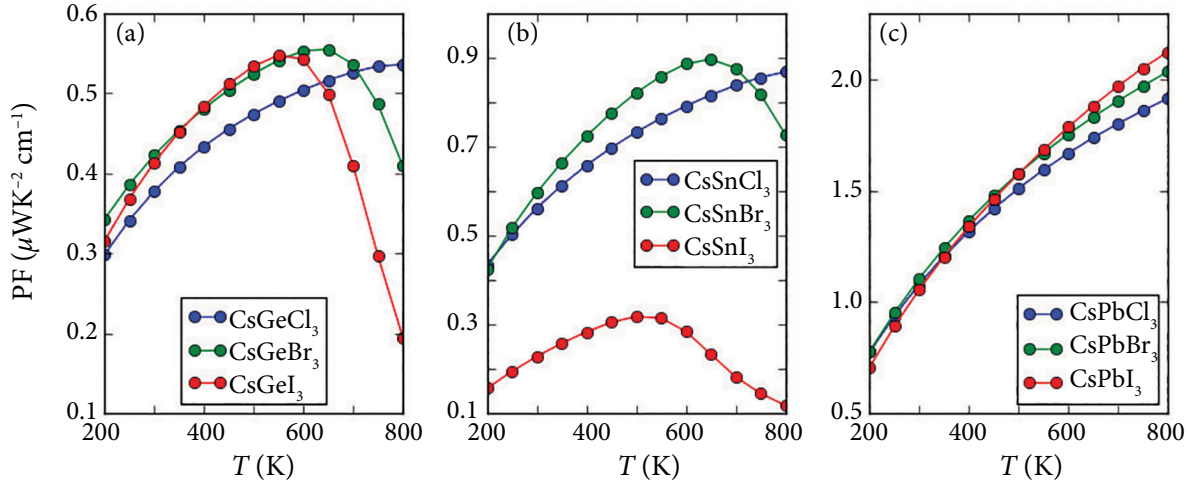


Fig. 6. Temperature-dependent power factor of $CsBX_3$ (B = Ge, Sn, Pb; X = Cl, Br, I).

to improve the competitiveness of thermoelectric material in directions other than $zT$. For example, efforts have focused on increasing the electrical power factor (PF). PF is an important thermoelectric parameter which relates the Seebeck coefficient and electrical conductivity by PF = $S\sigma^2$. Figure 6 depicts the $CsBX_3$ power factor as a function of temperature. In most of the considered temperature range, the power factor of lead-based compounds is considerably larger than that of the other

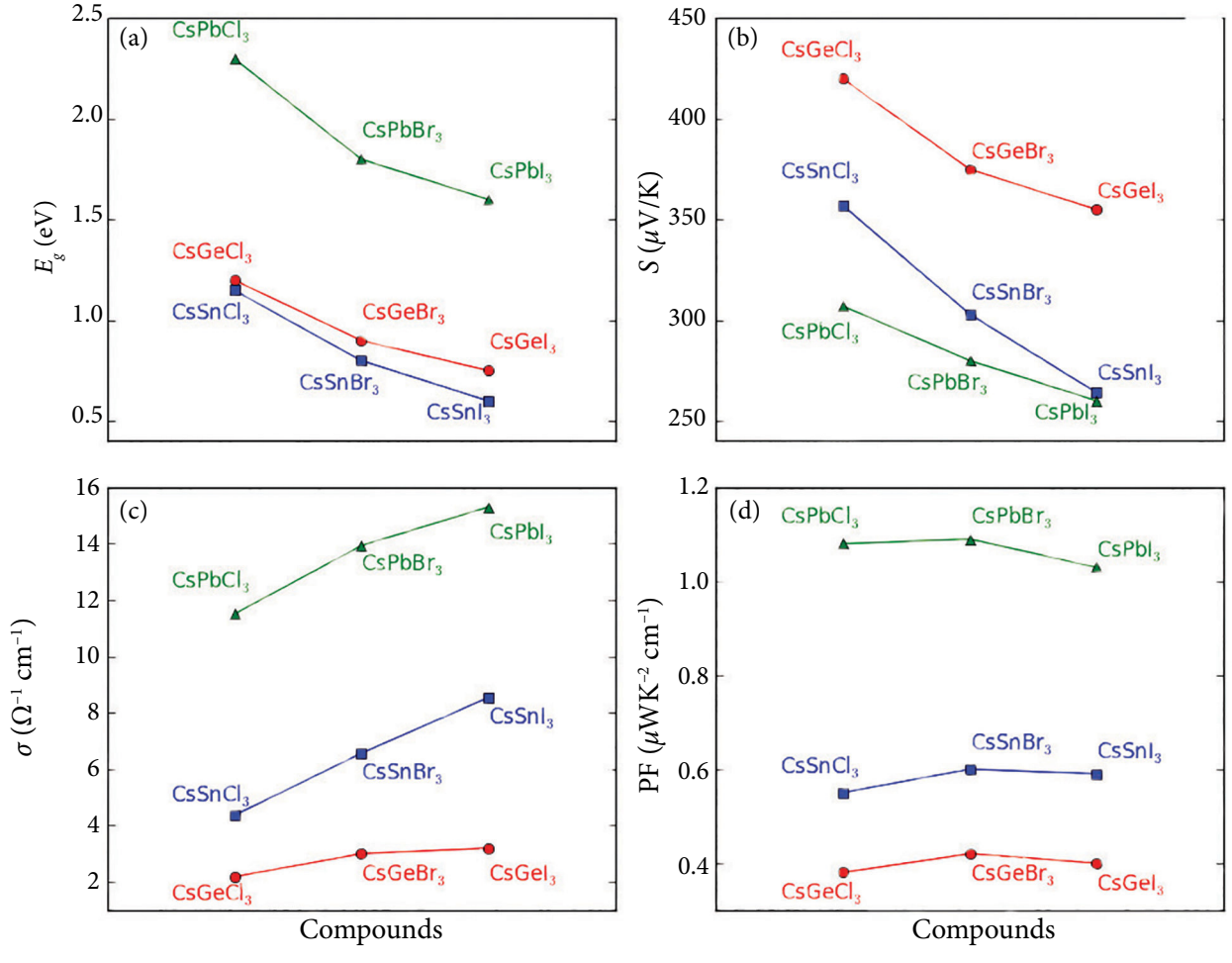


Fig. 7. The effect of replacement of halogen and metal cation atoms with other halogen and metal cation atoms on the electronic band gap (a), Seebeck coefficient (b), electrical conductivity (c) and power factor (d).

compounds (see Table 3). For $CsGeX_3$ $CsSnX_3$, according to the temperature increases, the power factor increases to reach its maxima at 600 K. Beyond the temperature of 600 K, a significant decrease is observed which is explained by a modification in the mobility of the electrons that corresponds to a change in the halide anions (iodine and bromine). This change is explained by the fact that PF follows the variations of the electrical conductivity. Our numerical data on band gap energy (Table 3) and other parameters of the investigated compounds (Table 3, at 300 K) are summarized graphically in Fig. 7. Figure 7(d) shows that the replacement of Pb by Sn or Ge causes a considerable reduction of PF. This is a general feature for most compounds and it is because of the change in atomic size and charge. The replacement of halogen atoms (Cl, Br, I) causes a slight variation in PF. Excluding lead-based compounds, our results suggest that $CsSnBr_3$ and $CsGeBr_3$ are prospective candidates for thermoelectric applications.

## 4. Conclusions

In summary, the structural, electronic and thermoelectric properties of metal halide cubic perovskites $CsBX_3$ (B = Ge, Sn, Pb and X = Cl, Br, I) are investigated using DFT and the Boltzmann transport equation. The effect of replacement of halogen and metal cation atoms by other halogen and metal cation atoms on electronic and thermoelectric properties is discussed. The lattice parameters and atomic positions are optimized. The electronic properties are determined through the calculation of the band structure as well as PDOS. We have determined the band gap and the contribution of each orbital in the atomic bonding of all $CsBX_3$ compounds. This study suggests that the electronic band gap value is affected due to the replacement of halogen and metal cation atoms. We also calculated the Seebeck coefficient, electrical conductivity and power factor of all $CsBX_3$ compounds. We have focused on the variations of thermoelectric properties as a function of atomic composition. Excluding lead-based compounds, our study shows that $CsSnBr_3$ and $CsGeBr_3$ compounds have the highest power factor. We suggest that the thermoelectric performance can be developed and tuned effectively with a good choice of chemical constituents of the compounds. This obtained result can be improved with new theoretical and experimental investigations, mainly to deepen our understanding of the effect of halogen and cation atoms on thermoelectric properties.

## References

[1] L. Zhang, X.-L. Shi, Y.-L. Yang, and Z.-G. Chen, Flexible thermoelectric materials and devices: From materials to applications, Mater. Today **46,** 62–108 (2021), https://doi.org/10.1016/j.mattod.2021.02.016

[2] M. Kaddes and M. Zemzemi, Computational study of electronic and thermoelectric properties of ZnO/graphene heterostructures, Int. J. Thermophys. **42**, 100 (2021), https://doi.org/10.1007/s10765-021-02854-5

[3] N. Kouaydi and M. Zemzemi, Electronic, band offset, and thermoelectric properties of ZnO/GaN heterostructure from first-principles study, J. Electron. Mater. **49**, 5773–5781 (2020), https://doi.org/10.1007/s11664-020-08341-1

[4] X. Wang, T. Zhang, Y. Lou, and Y. Zhao, All-inorganic lead-free perovskites for optoelectronic applications, Mater. Chem. Front. **3**, 365–375 (2019), https://doi.org/10.1039/C8QM00611C

[5] P. Zhang, J. Yang, and S.-H. Wei, Manipulation of cation combinations and configurations of halide double perovskites for solar cell absorbers, J. Mater. Chem. A **6**, 1809–1815 (2018), https://doi.org/10.1039/C7TA09713A

[6] H. Hu, B. Dong, and W. Zhang, Low-toxic metal halide perovskites: opportunities and future challenges, J. Mater. Chem. A **5**, 11436–11449 (2017), https://doi.org/10.1039/C7TA00269F

[7] G. Grancini and M.K. Nazeeruddin, Dimensional tailoring of hybrid perovskites for photovoltaics, Nat. Rev. Mater. **4**, 4–22 (2019), https://doi.org/10.1038/s41578-018-0065-0

[8] J. Burschka, N. Pellet, S.-J. Moon, R. Humphry-Baker, P. Gao, M.K. Nazeeruddin, and M. Grätzel, Sequential deposition as a route to high-performance perovskite-sensitized solar cells, Nature **499**, 316–319 (2013), https://doi.org/10.1038/nature12340

[9] H. Zhu, Y. Fu, F. Meng, X. Wu, Z. Gong, Q. Ding, M.V. Gustafsson, M.T. Trinh, S. Jin, and

X.-Y. Zhu, Lead halide perovskite nanowire lasers with low lasing thresholds and high quality factors, Nat. Mater. **14**, 636–642 (2015), https://doi.org/10.1038/nmat4271

[10] Gurudayal, D. Sabba, M.H. Kumar, L.H. Wong, J. Barber, M. Grätzel, and N. Mathews, Perovskite–hematite tandem cells for efficient overall solar driven water splitting, Nano Lett. **15**, 3833–3839 (2015), https://doi.org/10.1021/acs.nanolett.5b00616

[11] J. Luo, J.-H. Im, M.T. Mayer, M. Schreier, M.K. Nazeeruddin, N.-G. Park, S.D. Tilley, H.J. Fan, and M. Grätzel, Water photolysis at 12.3% efficiency via perovskite photovoltaics and earth-abundant catalysts, Science **345**, 1593–1596 (2014), https://doi.org/10.1126/science.1258307

[12] S.-T. Ha, C. Shen, J. Zhang, and Q. Xiong, Laser cooling of organic–inorganic lead halide perovskites, Nat. Photonics **10**, 115–121 (2016), https://doi.org/10.1038/nphoton.2015.243

[13] M. Méndez-Galván, B. Alcántar-Vázquez, G. Diaz, I.A. Ibarra, and H.A. Lara-García, Metal halide perovskites as an emergent catalyst for $CO_2$ photoreduction: a minireview, React. Chem. Eng. **6**, 828–838 (2021), https://doi.org/10.1039/D1RE00039J

[14] M. Li, R. Begum, J. Fu, Q. Xu, T.M. Koh, S.A. Veldhuis, M. Grätzel, N. Mathews, S. Mhaisalkar, and T.C. Sum, Low threshold and efficient multiple exciton generation in halide perovskite nanocrystals, Nat. Commun. **9**, 4197 (2018), https://doi.org/10.1038/s41467-018-06596-1

[15] S. Wei, Y. Yang, X. Kang, L. Wang, L. Huang, and D. Pan, Room-temperature and gram-scale synthesis of $CsPbX_3$ (X = Cl, Br, I) perovskite nanocrystals with 50–85% photoluminescence quantum yields, Chem. Commun. **52**, 7265–7268 (2016), https://doi.org/10.1039/C6CC01500J

[16] H. Xie, S. Hao, J. Bao, T.J. Slade, G.J. Snyder, C. Wolverton, and M.G. Kanatzidis, All-inorganic halide perovskites as potential thermoelectric materials: Dynamic cation off-centering induces ultralow thermal conductivity, J. Am. Chem. Soc. **142**, 9553–9563 (2020), https://doi.org/10.1021/jacs.0c03427

[17] M.S. Dresselhaus, G. Chen, M.Y. Tang, R.G. Yang, H. Lee, D.Z. Wang, Z.F. Ren, J.-P. Fleurial, and P. Gogna, New directions for low-dimensional thermoelectric materials, Adv. Mater. **19**, 1043–1053 (2007), https://doi.org/10.1002/adma.200600527

[18] S. Hu, Z. Ren, A.B. Djurišić, and A.L. Rogach, Metal halide perovskites as emerging thermoelectric materials, ACS Energy Lett. **6**, 3882–3905 (2021), https://doi.org/10.1021/acsenergylett.1c02015

[19] L.K. Ono, E.J. Juarez-Perez, and Y. Qi, Progress on perovskite materials and solar cells with mixed cations and halide anions, ACS Appl. Mater. Interfaces **9**, 30197–30246 (2017), https://doi.org/10.1021/acsami.7b06001

[20] G. Chen, M.S. Dresselhaus, G. Dresselhaus, J.-P. Fleurial, and T. Caillat, Recent developments in thermoelectric materials, Int. Mater. Rev. **48**, 45–66 (2003), https://doi.org/10.1179/095066003225010182

[21] J.-L. Calais, Book review: Density-functional theory of atoms and molecules. R.G. Parr and W. Yang, Oxford University Press, New York, Oxford, 1989. IX + 333 pp. Price £45.00, Int. J. Quantum Chem. **47**, 101–101 (1993), https://doi.org/10.1002/qua.560470107

[22] X. Gonze, B. Amadon, P.-M. Anglade, J.-M. Beuken, F. Bottin, P. Boulanger, F. Bruneval, D. Caliste, R. Caracas, M. Côté, et al., ABINIT: First-principles approach to material and nanosystem properties, Comput. Phys. Commun. **180**, 2582–2615 (2009), https://doi.org/10.1016/j.cpc.2009.07.007

[23] K.F. Garrity, J.W. Bennett, K.M. Rabe, and D. Vanderbilt, Pseudopotentials for high-throughput DFT calculations, Comput. Mater. Sci. **81**, 446–452 (2014), https://doi.org/10.1016/j.commatsci.2013.08.053

[24] P.E. Blöchl, Projector augmented-wave method, Phys. Rev. B **50**, 17953–17979 (1994), https://doi.org/10.1103/PhysRevB.50.17953

[25] H.J. Monkhorst and J.D. Pack, Special points for Brillouin-zone integrations, Phys. Rev. B **13**, 5188–5192 (1976), https://doi.org/10.1103/PhysRevB.13.5188

[26] M. Hebbache and M. Zemzemi, *Ab initio* study of high-pressure behavior of a low compressibility metal and a hard material: Osmium and diamond, Phys. Rev. B **70**, 224107 (2004), https://doi.org/10.1103/PhysRevB.70.224107

[27] G.K.H. Madsen and D.J. Singh, BoltzTraP. A code for calculating band-structure dependent quantities, Comput. Phys. Commun. **175**, 67–71 (2006), https://doi.org/10.1016/j.cpc.2006.03.007

[28] T.J. Scheidemantel, C. Ambrosch-Draxl, T. Thonhauser, J.V. Badding, and J.O. Sofo, Transport coefficients from first-principles calculations, Phys. Rev. B **68**, 125210 (2003), https://doi.org/10.1103/PhysRevB.68.125210

[29] R.X. Yang, J.M. Skelton, E.L. da Silva, J.M. Frost, and A. Walsh, Assessment of dynamic structural instabilities across 24 cubic inorganic halide perovskites, J. Chem. Phys. **152**, 024703 (2020), https://doi.org/10.1063/1.5131575

[30] R.W.G. Wyckoff, *The Structure of Crystals* (Chemical Catalog Company, 1931), https://books.google.tn/books?id=bcvRAAAAMAAJ

[31] M.G. Brik, Comparative first-principles calculations of electronic, optical and elastic anisotropy properties of $CsXBr_3$ (X = Ca, Ge, Sn) crystals, Solid State Commun. **151**, 1733–1738 (2011), https://doi.org/10.1016/j.ssc.2011.08.039

[32] G. Thiele, H.W. Rotter, and K.D. Schmidt, Kristallstrukturen und Phasentransformationen von Caesiumtrihalogenogermanaten(II) $CsGeX_3$ (X = Cl, Br, I), Z. Anorg. Allg. Chem. **545**, 148–156 (1987), https://doi.org/10.1002/zaac.19875450217

[33] J. Barrett, S.R.A. Bird, J.D. Donaldson, and J. Silver, The Mössbauer effect in tin(II) compounds. Part XI. The spectra of cubic trihalogenostannates(II), J. Chem. Soc. A **0**, 3105–3108 (1971), https://doi.org/10.1039/J19710003105

[34] A.K. Deb and V. Kumar, *Ab initio* design of $CsSn(X_xY_{1-x})_3$ (X and Y = Cl, Br, and I) perovskites for photovoltaics, AIP Adv. **5**, 077158 (2015), https://doi.org/10.1063/1.4927503

[35] S. Hébert, D. Flahaut, C. Martin, S. Lemonnier, J. Noudem, C. Goupil, A. Maignan, and J. Hejtmanek, Thermoelectric properties of perovskites: Sign change of the Seebeck coefficient and high temperature properties, Prog. Solid State Chem. **35**, 457–467 (2007), https://doi.org/10.1016/j.progsolidstchem.2007.01.027

[36] K. Yamada, S. Funabiki, H. Horimoto, T. Matsui, T. Okuda, and S. Ichiba, Structural phase transitions of the polymorphs of $CsSnI_3$ by means of Rietveld analysis of the X-ray diffraction, Chem. Lett. **20**, 801–804 (1991), https://doi.org/10.1246/cl.1991.801

[37] L. Lang, J.-H. Yang, H.-R. Liu, H.J. Xiang, and X.G. Gong, First-principles study on the electronic and optical properties of cubic $ABX_3$ halide perovskites, Phys. Lett. A **378**, 290–293 (2014), https://doi.org/10.1016/j.physleta.2013.11.018

[38] M. Ahmad, G. Rehman, L. Ali, M. Shafiq, R. Iqbal, R. Ahmad, T. Khan, S. Jalali-Asadabadi, M. Maqbool, and I. Ahmad, Structural, electronic and optical properties of $CsPbX_3$ (X = Cl, Br, I) for energy storage and hybrid solar cell applications, J. Alloys Compd. **705**, 828–839 (2017), https://doi.org/10.1016/j.jallcom.2017.02.147

[39] H.M. Ghaithan, Z.A. Alahmed, A. Lyras, S.M.H. Qaid, and A.S. Aldwayyan, Computational investigation of the folded and unfolded band structure and structural and optical properties of $CsPb(I_{1-x}Br_x)_3$ perovskites, Crystals **10**, 342 (2020), https://doi.org/10.3390/cryst10050342

[40] R.E. Beal, D.J. Slotcavage, T. Leijtens, A.R. Bowring, R.A. Belisle, W.H. Nguyen, G.F. Burkhard, E.T. Hoke, and M.D. McGehee, Cesium lead halide perovskites with improved stability for tandem solar cells, J. Phys. Chem. Lett. **7**, 746–751 (2016), https://doi.org/10.1021/acs.jpclett.6b00002

[41] L. Protesescu, S. Yakunin, M.I. Bodnarchuk, F. Krieg, R. Caputo, C.H. Hendon, R.X. Yang, A. Walsh, and M.V. Kovalenko, Nanocrystals of cesium lead halide perovskites ($CsPbX_3$, X = Cl, Br, and I): Novel optoelectronic materials showing bright emission with wide color gamut, Nano Lett. **15**, 3692–3696 (2015), https://doi.org/10.1021/nl5048779

[42] S. Körbel, M.A.L. Marques, and S. Botti, Stability and electronic properties of new inorganic perovskites from high-throughput *ab initio* calculations, J. Mater. Chem. C **4**, 3157–3167 (2016), https://doi.org/10.1039/C5TC04172D

[43] M. Roknuzzaman, K. Ostrikov, H. Wang, A. Du, and T. Tesfamichael, Towards lead-free perovskite photovoltaics and optoelectronics by *ab-initio* simulations, Sci. Rep. **7**, 14025 (2017), https://doi.org/10.1038/s41598-017-13172-y

[44] Z.-G. Lin, L.-C. Tang, and C.-P. Chou, Study on mid-IR NLO crystals $CsGe(Br_xCl_{1-x})_3$, Opt. Mater. **31**, 28–34 (2008), https://doi.org/10.1016/j.optmat.2008.01.004

[45] T. Krishnamoorthy, H. Ding, C. Yan, W.L. Leong, T. Baikie, Z. Zhang, M. Sherburne, S. Li, M. Asta, N. Mathews, and S.G. Mhaisalkar, Lead-free germanium iodide perovskite materials for photovoltaic applications, J. Mater. Chem. A **3**, 23829–23832 (2015), https://doi.org/10.1039/C5TA05741H

[46] A.S. Voloshinovskii, S.V. Myagkota, N.S. Pidzyrailo, and M.V. Tokarivskii, Luminescence and structural transformations of $CsSnCl_3$ crystals, J. Appl. Spectrosc. **60**, 226–228 (1994), https://doi.org/10.1007/BF02606360

[47] C. Yu, Z. Chen, J.J. Wang, W. Pfenninger, N. Vockic, J.T. Kenney, and K. Shum, Temperature dependence of the band gap of perovskite semiconductor compound $CsSnI_3$, J. Appl. Phys. **110**, 063526 (2011), https://doi.org/10.1063/1.3638699

[48] A. Filippetti, C. Caddeo, P. Delugas, and A. Mattoni, Appealing perspectives of hybrid lead–iodide perovskites as thermoelectric materials, J. Phys. Chem. C **120**, 28472–28479 (2016), https://doi.org/10.1021/acs.jpcc.6b10278

[49] Y. Liu, D. Cadavid, M. Ibáñez, S. Ortega, S. Martí-Sánchez, O. Dobrozhan, M.V. Kovalenko, J. Arbiol, and A. Cabot, Thermoelectric properties of semiconductor-metal composites produced by particle blending, APL Mater. **4**, 104813 (2016), https://doi.org/10.1063/1.4961679

## METALO HALIDO KUBINIŲ PEROVSKITŲ $CsBX_3$ (B = Ge, Sn, Pb IR X = Cl, Br, I) ELEKTRONINIŲ IR TERMOELEKTRINIŲ SAVYBIŲ SKAIČIAVIMAI

M. Zemzemi

*Gabeso universiteto Mokslų fakultetas, Gabesas, Tunisas*